Measurement of inelastic J/ψ and ψ' photoproduction at HERA

ZEUS Collaboration

Abstract

The cross sections for inelastic photoproduction of J/ψ and ψ' mesons have been measured in ep collisions with the ZEUS detector at HERA, using an integrated luminosity of 468 pb^{-1} collected in the period 1996–2007. The ψ' to J/ψ cross section ratio was measured in the range $0.55 < z < 0.9$ and $60 < W < 190\,\mathrm{GeV}$ as a function of W, z and p_T. Here W denotes the photon-proton centre-of-mass energy, z is the fraction of the incident photon energy carried by the meson and p_T is the transverse momentum of the meson with respect to the beam axis. The J/ψ cross sections were measured for $0.1 < z < 0.9$, $60 < W < 240\,\mathrm{GeV}$ and $p_T > 1\,\mathrm{GeV}$. Theoretical predictions within the non-relativistic QCD framework including NLO colour–singlet and colour–octet contributions were compared to the data, as were predictions based on the k_T–factorisation approach.

The ZEUS Collaboration

H. Abramowicz[45,ah], I. Abt[35], L. Adamczyk[13], M. Adamus[54], R. Aggarwal[7,c], S. Antonelli[4], P. Antonioli[3], A. Antonov[33], M. Arneodo[50], O. Arslan[5], V. Aushev[26,27,aa], Y. Aushev,[27,aa,ab], O. Bachynska[15], A. Bamberger[19], A.N. Barakbaev[25], G. Barbagli[17], G. Bari[3], F. Barreiro[30], N. Bartosik[15], D. Bartsch[5], M. Basile[4], O. Behnke[15], J. Behr[15], U. Behrens[15], L. Bellagamba[3], A. Bertolin[39], S. Bhadra[57], M. Bindi[4], C. Blohm[15], V. Bokhonov[26,aa], T. Bołd[13], K. Bondarenko[27], E.G. Boos[25], K. Borras[15], D. Boscherini[3], D. Bot[15], I. Brock[5], E. Brownson[56], R. Brugnera[40], N. Brümmer[37], A. Bruni[3], G. Bruni[3], B. Brzozowska[53], P.J. Bussey[20], B. Bylsma[37], A. Caldwell[35], M. Capua[8], R. Carlin[40], C.D. Catterall[57], S. Chekanov[1], J. Chwastowski[12,e], J. Ciborowski[53,al], R. Ciesielski[15,h], L. Cifarelli[4], F. Cindolo[3], A. Contin[4], A.M. Cooper-Sarkar[38], N. Coppola[15,i], M. Corradi[3], F. Corriveau[31], M. Costa[49], G. D'Agostini[43], F. Dal Corso[39], J. del Peso[30], R.K. Dementiev[34], S. De Pasquale[4,a], M. Derrick[1], R.C.E. Devenish[38], D. Dobur[19,u], B.A. Dolgoshein [33,†], G. Dolinska[27], A.T. Doyle[20], V. Drugakov[16], L.S. Durkin[37], S. Dusini[39], Y. Eisenberg[55], P.F. Ermolov [34,†], A. Eskreys [12,†], S. Fang[15,j], S. Fazio[8], J. Ferrando[20], M.I. Ferrero[49], J. Figiel[12], B. Foster[38,ad], G. Gach[13], A. Galas[12], E. Gallo[17], A. Garfagnini[40], A. Geiser[15], I. Gialas[21,x], A. Gizhko[27,ac], L.K. Gladilin[34], D. Gladkov[33], C. Glasman[30], O. Gogota[27], Yu.A. Golubkov[34], P. Göttlicher[15,k], I. Grabowska-Bołd[13], J. Grebenyuk[15], I. Gregor[15], G. Grigorescu[36], G. Grzelak[53], O. Gueta[45], M. Guzik[13], C. Gwenlan[38,ae], T. Haas[15], W. Hain[15], R. Hamatsu[48], J.C. Hart[44], H. Hartmann[5], G. Hartner[57], E. Hilger[5], D. Hochman[55], R. Hori[47], A. Hüttmann[15], Z.A. Ibrahim[10], Y. Iga[42], R. Ingbir[45], M. Ishitsuka[46], H.-P. Jakob[5], F. Januschek[15], T.W. Jones[52], M. Jüngst[5], I. Kadenko[27], B. Kahle[15], S. Kananov[45], T. Kanno[46], U. Karshon[55], F. Karstens[19,v], I.I. Katkov[15,l], M. Kaur[7], P. Kaur[7,c], A. Keramidas[36], L.A. Khein[34], J.Y. Kim[9], D. Kisielewska[13], S. Kitamura[48,aj], R. Klanner[22], U. Klein[15,m], E. Koffeman[36], N. Kondrashova[27,ac], O. Kononenko[27], P. Kooijman[36], Ie. Korol[27], I.A. Korzhavina[34], A. Kotański[14,f], U. Kötz[15], H. Kowalski[15], O. Kuprash[15], M. Kuze[46], A. Lee[37], B.B. Levchenko[34], A. Levy[45], V. Libov[15], S. Limentani[40], T.Y. Ling[37], M. Lisovyi[15], E. Lobodzinska[15], W. Lohmann[16], B. Löhr[15], E. Lohrmann[22], K.R. Long[23], A. Longhin[39,af], D. Lontkovskyi[15], O.Yu. Lukina[34], J. Maeda[46,ai], S. Magill[1], I. Makarenko[15], J. Malka[15], R. Mankel[15], A. Margotti[3], G. Marini[43], J.F. Martin[51], A. Mastroberardino[8], M.C.K. Mattingly[2], I.-A. Melzer-Pellmann[15], S. Mergelmeyer[5], S. Miglioranzi[15,n], F. Mohamad Idris[10], V. Monaco[49], A. Montanari[15], J.D. Morris[6,b], K. Mujkic[15,o], B. Musgrave[1], K. Nagano[24], T. Namsoo[15,p], R. Nania[3], A. Nigro[43], Y. Ning[11], T. Nobe[46], D. Notz[15], R.J. Nowak[53], A.E. Nuncio-Quiroz[5], B.Y. Oh[41], N. Okazaki[47], K. Olkiewicz[12], Yu. Onishchuk[27], K. Papageorgiu[21], A. Parenti[15], E. Paul[5], J.M. Pawlak[53], B. Pawlik[12], P. G. Pelfer[18], A. Pellegrino[36], W. Perlański[53,am], H. Perrey[15], K. Piotrzkowski[29], P. Pluciński[54,an], N.S. Pokrovskiy[25], A. Polini[3], A.S. Proskuryakov[34], M. Przybycień[13], A. Raval[15], D.D. Reeder[56], B. Reisert[35], Z. Ren[11], J. Repond[1], Y.D. Ri[48,ak], A. Robertson[38], P. Roloff[15,n], I. Rubinsky[15], M. Ruspa[50], R. Sacchi[49], U. Samson[5], G. Sartorelli[4], A.A. Savin[56], D.H. Saxon[20], M. Schioppa[8], S. Schlenstedt[16], P. Schleper[22], W.B. Schmidke[35], U. Schneekloth[15], V. Schönberg[5], T. Schörner-Sadenius[15], J. Schwartz[31], F. Sciulli[11], L.M. Shcheglova[34], R. Shehzadi[5], S. Shimizu[47,n], I. Singh[7,c], I.O. Skillicorn[20], W. Słomiński[14,g], W.H. Smith[56], V. Sola[22], A. Solano[49], D. Son[28],

V. Sosnovtsev[33], A. Spiridonov[15,q], H. Stadie[22], L. Stanco[39], N. Stefaniuk[27], A. Stern[45], T.P. Stewart[51], A. Stifutkin[33], P. Stopa[12], S. Suchkov[33], G. Susinno[8], L. Suszycki[13], J. Sztuk-Dambietz[22], D. Szuba[22], J. Szuba[15,r], A.D. Tapper[23], E. Tassi[8,d], J. Terrón[30], T. Theedt[15], H. Tiecke[36], K. Tokushuku[24,y], J. Tomaszewska[15,s], V. Trusov[27], T. Tsurugai[32], M. Turcato[22], O. Turkot[27,ac], T. Tymieniecka[54,ao], M. Vázquez[36,n], A. Verbytskyi[15], O. Viazlo[27], N.N. Vlasov[19,w], R. Walczak[38], W.A.T. Wan Abdullah[10], J.J. Whitmore[41,ag], K. Wichmann[15,t], L. Wiggers[36], M. Wing[52], M. Wlasenko[5], G. Wolf[15], H. Wolfe[56], K. Wrona[15], A.G. Yagües-Molina[15], S. Yamada[24], Y. Yamazaki[24,z], R. Yoshida[1], C. Youngman[15], O. Zabiegalov[27,ac], A.F. Żarnecki[53], L. Zawiejski[12], O. Zenaiev[15], W. Zeuner[15,n], B.O. Zhautykov[25], N. Zhmak[26,aa], A. Zichichi[4], Z. Zolkapli[10], D.S. Zotkin[34]

[1] *Argonne National Laboratory, Argonne, Illinois 60439-4815, USA* [A]
[2] *Andrews University, Berrien Springs, Michigan 49104-0380, USA*
[3] *INFN Bologna, Bologna, Italy* [B]
[4] *University and INFN Bologna, Bologna, Italy* [B]
[5] *Physikalisches Institut der Universität Bonn, Bonn, Germany* [C]
[6] *H.H. Wills Physics Laboratory, University of Bristol, Bristol, United Kingdom* [D]
[7] *Panjab University, Department of Physics, Chandigarh, India*
[8] *Calabria University, Physics Department and INFN, Cosenza, Italy* [B]
[9] *Institute for Universe and Elementary Particles, Chonnam National University, Kwangju, South Korea*
[10] *Jabatan Fizik, Universiti Malaya, 50603 Kuala Lumpur, Malaysia* [E]
[11] *Nevis Laboratories, Columbia University, Irvington on Hudson, New York 10027, USA* [F]
[12] *The Henryk Niewodniczanski Institute of Nuclear Physics, Polish Academy of Sciences, Krakow, Poland* [G]
[13] *AGH-University of Science and Technology, Faculty of Physics and Applied Computer Science, Krakow, Poland* [H]
[14] *Department of Physics, Jagellonian University, Cracow, Poland*
[15] *Deutsches Elektronen-Synchrotron DESY, Hamburg, Germany*
[16] *Deutsches Elektronen-Synchrotron DESY, Zeuthen, Germany*
[17] *INFN Florence, Florence, Italy* [B]
[18] *University and INFN Florence, Florence, Italy* [B]
[19] *Fakultät für Physik der Universität Freiburg i.Br., Freiburg i.Br., Germany*
[20] *School of Physics and Astronomy, University of Glasgow, Glasgow, United Kingdom* [D]
[21] *Department of Engineering in Management and Finance, Univ. of the Aegean, Chios, Greece*
[22] *Hamburg University, Institute of Experimental Physics, Hamburg, Germany* [I]
[23] *Imperial College London, High Energy Nuclear Physics Group, London, United Kingdom* [D]
[24] *Institute of Particle and Nuclear Studies, KEK, Tsukuba, Japan* [J]
[25] *Institute of Physics and Technology of Ministry of Education and Science of Kazakhstan, Almaty, Kazakhstan*
[26] *Institute for Nuclear Research, National Academy of Sciences, Kyiv, Ukraine*
[27] *Department of Nuclear Physics, National Taras Shevchenko University of Kyiv, Kyiv, Ukraine*
[28] *Kyungpook National University, Center for High Energy Physics, Daegu, South Korea* [K]
[29] *Institut de Physique Nucléaire, Université Catholique de Louvain, Louvain-la-Neuve, Belgium* [L]
[30] *Departamento de Física Teórica, Universidad Autónoma de Madrid, Madrid, Spain* [M]

[31] *Department of Physics, McGill University, Montréal, Québec, Canada H3A 2T8* [N]
[32] *Meiji Gakuin University, Faculty of General Education, Yokohama, Japan* [J]
[33] *Moscow Engineering Physics Institute, Moscow, Russia* [O]
[34] *Lomonosov Moscow State University, Skobeltsyn Institute of Nuclear Physics, Moscow, Russia* [P]
[35] *Max-Planck-Institut für Physik, München, Germany*
[36] *NIKHEF and University of Amsterdam, Amsterdam, Netherlands* [Q]
[37] *Physics Department, Ohio State University, Columbus, Ohio 43210, USA* [A]
[38] *Department of Physics, University of Oxford, Oxford, United Kingdom* [D]
[39] *INFN Padova, Padova, Italy* [B]
[40] *Dipartimento di Fisica dell' Università and INFN, Padova, Italy* [B]
[41] *Department of Physics, Pennsylvania State University, University Park, Pennsylvania 16802, USA* [F]
[42] *Polytechnic University, Tokyo, Japan* [J]
[43] *Dipartimento di Fisica, Università 'La Sapienza' and INFN, Rome, Italy* [B]
[44] *Rutherford Appleton Laboratory, Chilton, Didcot, Oxon, United Kingdom* [D]
[45] *Raymond and Beverly Sackler Faculty of Exact Sciences, School of Physics, Tel Aviv University, Tel Aviv, Israel* [R]
[46] *Department of Physics, Tokyo Institute of Technology, Tokyo, Japan* [J]
[47] *Department of Physics, University of Tokyo, Tokyo, Japan* [J]
[48] *Tokyo Metropolitan University, Department of Physics, Tokyo, Japan* [J]
[49] *Università di Torino and INFN, Torino, Italy* [B]
[50] *Università del Piemonte Orientale, Novara, and INFN, Torino, Italy* [B]
[51] *Department of Physics, University of Toronto, Toronto, Ontario, Canada M5S 1A7* [N]
[52] *Physics and Astronomy Department, University College London, London, United Kingdom* [D]
[53] *Faculty of Physics, University of Warsaw, Warsaw, Poland*
[54] *National Centre for Nuclear Research, Warsaw, Poland*
[55] *Department of Particle Physics and Astrophysics, Weizmann Institute, Rehovot, Israel*
[56] *Department of Physics, University of Wisconsin, Madison, Wisconsin 53706, USA* [A]
[57] *Department of Physics, York University, Ontario, Canada M3J 1P3* [N]

[A] supported by the US Department of Energy
[B] supported by the Italian National Institute for Nuclear Physics (INFN)
[C] supported by the German Federal Ministry for Education and Research (BMBF), under contract No. 05 H09PDF
[D] supported by the Science and Technology Facilities Council, UK
[E] supported by HIR and UMRG grants from Universiti Malaya, and an ERGS grant from the Malaysian Ministry for Higher Education
[F] supported by the US National Science Foundation. Any opinion, findings and conclusions or recommendations expressed in this material are those of the authors and do not necessarily reflect the views of the National Science Foundation.
[G] supported by the Polish Ministry of Science and Higher Education as a scientific project No. DPN/N188/DESY/2009
[H] supported by the Polish Ministry of Science and Higher Education and its grants for Scientific Research
[I] supported by the German Federal Ministry for Education and Research (BMBF), under contract No. 05h09GUF, and the SFB 676 of the Deutsche Forschungsgemeinschaft (DFG)
[J] supported by the Japanese Ministry of Education, Culture, Sports, Science and Technology (MEXT) and its grants for Scientific Research
[K] supported by the Korean Ministry of Education and Korea Science and Engineering Foundation
[L] supported by FNRS and its associated funds (IISN and FRIA) and by an Inter-University Attraction Poles Programme subsidised by the Belgian Federal Science Policy Office
[M] supported by the Spanish Ministry of Education and Science through funds provided by CICYT
[N] supported by the Natural Sciences and Engineering Research Council of Canada (NSERC)
[O] partially supported by the German Federal Ministry for Education and Research (BMBF)
[P] supported by RF Presidential grant N 3920.2012.2 for the Leading Scientific Schools and by the Russian Ministry of Education and Science through its grant for Scientific Research on High Energy Physics
[Q] supported by the Netherlands Foundation for Research on Matter (FOM)
[R] supported by the Israel Science Foundation

[a] now at University of Salerno, Italy
[b] now at Queen Mary University of London, United Kingdom
[c] also funded by Max Planck Institute for Physics, Munich, Germany
[d] also Senior Alexander von Humboldt Research Fellow at Hamburg University, Institute of Experimental Physics, Hamburg, Germany
[e] also at Cracow University of Technology, Faculty of Physics, Mathemathics and Applied Computer Science, Poland
[f] supported by the research grant No. 1 P03B 04529 (2005-2008)
[g] partially supported by the Polish National Science Centre projects DEC-2011/01/B/ST2/03643 and DEC-2011/03/B/ST2/00220
[h] now at Rockefeller University, New York, NY 10065, USA
[i] now at DESY group FS-CFEL-1
[j] now at Institute of High Energy Physics, Beijing, China
[k] now at DESY group FEB, Hamburg, Germany
[l] also at Moscow State University, Russia
[m] now at University of Liverpool, United Kingdom
[n] now at CERN, Geneva, Switzerland
[o] also affiliated with Universtiy College London, UK
[p] now at Goldman Sachs, London, UK
[q] also at Institute of Theoretical and Experimental Physics, Moscow, Russia
[r] also at FPACS, AGH-UST, Cracow, Poland
[s] partially supported by Warsaw University, Poland
[t] supported by the Alexander von Humboldt Foundation
[u] now at Istituto Nucleare di Fisica Nazionale (INFN), Pisa, Italy
[v] now at Haase Energie Technik AG, Neumünster, Germany
[w] now at Department of Physics, University of Bonn, Germany
[x] also affiliated with DESY, Germany
[y] also at University of Tokyo, Japan
[z] now at Kobe University, Japan
[†] deceased
[aa] supported by DESY, Germany
[ab] member of National Technical University of Ukraine, Kyiv Polytechnic Institute, Kyiv, Ukraine
[ac] member of National University of Kyiv - Mohyla Academy, Kyiv, Ukraine
[ad] Alexander von Humboldt Professor; also at DESY and University of Oxford
[ae] STFC Advanced Fellow
[af] now at LNF, Frascati, Italy
[ag] This material was based on work supported by the National Science Foundation, while working at the Foundation.
[ah] also at Max Planck Institute for Physics, Munich, Germany, External Scientific Member

[ai] now at Tokyo Metropolitan University, Japan
[aj] now at Nihon Institute of Medical Science, Japan
[ak] now at Osaka University, Osaka, Japan
[al] also at Łódź University, Poland
[am] member of Łódź University, Poland
[an] now at Department of Physics, Stockholm University, Stockholm, Sweden
[ao] also at Cardinal Stefan Wyszyński University, Warsaw, Poland

1 Introduction

The inelastic production of J/ψ and of ψ' has been studied for several years in hadron and electron-proton colliders and in fixed target experiments [1]. At HERA, the reactions

$$ep \to eJ/\psi X, \tag{1}$$

and

$$ep \to e\psi' X, \tag{2}$$

have been studied [2, 3] for low virtuality of the exchanged photon (photoproduction) in the range $z < 0.9$, where z denotes the fraction of the incident photon energy carried by the meson in the proton rest frame, thus excluding the diffractive process for which $z \sim 1$. In the HERA photoproduction regime, the production of inelastic J/ψ or ψ' mesons arises mostly from direct and resolved photon interactions. In leading-order (LO) Quantum Chromodynamics (QCD), the two processes can be distinguished; in direct-photon processes the photon enters directly into the hard interaction; in resolved-photon processes the photon acts as a source of partons, one of which participates in the hard interaction. The inelastic process in the photoproduction region is dominated by photon–gluon fusion. In this direct-photon process the photon emitted from the incoming electron interacts with a gluon from the proton to produce a pair of charm-anticharm quarks, $c\bar{c}$, which then turn into the J/ψ or the ψ' mesons. When the $c\bar{c}$ pair emerges from the hard process with the quantum numbers of the mesons, the reaction is described in the framework of perturbative Quantum Chromodynamics (pQCD) by models such as the Colour Singlet (CS) model. In the Colour Octet (CO) model, the $c\bar{c}$ pair emerges from the hard process with quantum numbers different from those of the mesons and emits one or more soft gluons before turning into the physical meson state. Examples of direct-photon LO diagrams with a CS and a CO hard subprocess are shown in Fig. 1.

Full next-to-leading order (NLO) J/ψ cross section predictions using only the direct-photon CS contributions have already been performed [4, 5]. The non-relativistic QCD framework (NRQCD) [6] allows the evaluation of J/ψ cross sections including direct and resolved photon processes with CS and CO contributions. The former contribution can be thought of as the first term of the NRQCD expansion and so it is an integral component of this theoretical formalism. Recently, the full computation was performed in the HERA photoproduction regime at the NLO level [7]. The numerical values of the CS and CO matrix elements were obtained from a global fit to hadroproduction, electroproduction and photoproduction inelastic J/ψ data [7].

J/ψ cross sections have also been evaluated [8, 9] in the k_T–factorisation approach [10]. In this model, based on non–collinear parton dynamics governed by the CCFM [11] evolution equations, effects of non–zero gluon transverse momentum are taken into account. Cross sections are then calculated as the convolution of unintegrated, transverse–momentum dependent gluon densities and LO off–shell matrix elements. Direct and resolved photon processes are included. The matrix elements are computed in the CS model.

Measurements of the reactions (1) and (2) have been previously performed by the ZEUS collaboration [2], using an integrated luminosity of 38 pb^{-1}, and by the H1 collaboration [3], using an integrated luminosity of 165 pb^{-1}. Total and differential cross sections were presented as a function of various kinematical variables. The H1 and ZEUS collaborations have also published a measurement of the J/ψ helicity distribution [3, 12], the ZEUS result was obtained using the full HERA luminosity. LO and NLO QCD predictions, as well as LO NRQCD calculations, were compared to the measurements. None of the calculations could describe the data in the whole kinematic range of the measurements. The data were shown to have the potential to reduce the large uncertainties in the phenomenological parameters used in the calculations.

In this paper, measurements of reactions (1) and (2) are presented using a luminosity of 468 pb^{-1}. The J/ψ and ψ' mesons were identified using the $\mu^+\mu^-$ decay modes.

The ψ' to J/ψ cross section ratio was measured in the range $60 < W < 190$ GeV and $0.55 < z < 0.9$ as a function of W, z and p_T. Here W is the γp centre-of-mass energy and p_T is the transverse momentum of the mesons with respect to the beam axis. The cross sections for inelastic J/ψ photoproduction as a function of p_T^2, for different z ranges, and as a function of z, for different p_T ranges, were measured in the range $60 < W < 240$ GeV, $0.1 < z < 0.9$ and $p_T > 1$ GeV. The momentum flow along and against the J/ψ direction of flight in the laboratory frame, as obtained from the charged tracks produced together with the J/ψ in the range $60 < W < 240$ GeV, $0.3 < z < 0.9$ and $1 < p_T < 10$ GeV, was studied in order to shed further light on the production mechanisms.

2 Experimental set-up

The analysis presented here is based on data collected by the ZEUS detector at HERA in the period 1996–2007. In 1998–2007 (1996–1997), HERA provided electron[1] beams of

[1]Here and in the following, the term "electron" denotes generically both the electron (e^-) and the positron (e^+).

energy $E_e = 27.5$ GeV and proton beams of energy $E_p = 920$ (820) GeV, resulting in a centre-of-mass energy of $\sqrt{s} = 318$ (300) GeV, giving an integrated luminosity of 430 (38) pb^{-1}.

A detailed description of the ZEUS detector can be found elsewhere [13,14]. A brief outline of the components that are most relevant for this analysis is given below.

Charged particles were tracked in the central tracking detector (CTD) [15], which operated in a magnetic field of 1.43 T provided by a thin superconducting coil. Before the 2003–2007 running period, the ZEUS tracking system was upgraded with a silicon microvertex detector (MVD) [16]. In the following, the term "CTD-MVD track" denotes generically both the tracks measured in the CTD and (after 2002) in the CTD and MVD.

The high-resolution uranium–scintillator calorimeter (CAL) [17] consisted of three parts: the forward (FCAL), the barrel (BCAL) and the rear (RCAL) calorimeters[2]. Each part was subdivided transversely into towers and longitudinally into one electromagnetic section (EMC) and either one (in RCAL) or two (in BCAL and FCAL) hadronic sections (HAC). The smallest subdivision of the calorimeter was called a cell. The CAL energy resolutions, as measured under test-beam conditions, were $\sigma(E)/E = 0.18/\sqrt{E}$ for electrons and $\sigma(E)/E = 0.35/\sqrt{E}$ for hadrons (E in GeV). The timing resolution of the CAL was better than 1 ns for energy deposits greater than 4.5 GeV.

Muons were identified as tracks measured in the barrel and rear muon chambers (BMUON and RMUON) [18]. The muon chambers were placed inside and outside the magnetised iron yoke surrounding the CAL. The barrel and rear inner muon chambers (BMUI and RMUI) covered the polar-angle regions $34^\circ < \theta < 135^\circ$ and $135^\circ < \theta < 171^\circ$, respectively.

The luminosity was measured using the Bethe–Heitler reaction $ep \to e\gamma p$ with the luminosity detector which consisted of a lead–scintillator calorimeter [19] and, after 2002, of an additional magnetic spectrometer [20] system. The fractional systematic uncertainty on the measured luminosity was 1.9%.

[2] The ZEUS coordinate system is a right-handed Cartesian system, with the Z axis pointing in the proton–beam direction, referred to as the "forward direction", and the X axis pointing towards the centre of HERA. The coordinate origin is at the nominal interaction point. The polar angle, θ, is measured with respect to the proton–beam direction. The pseudorapidity is defined as η=–ln(tan $\frac{\theta}{2}$).

3 Event selection and kinematic variables

The online and offline selections, as well as the reconstruction of the kinematic variables, closely follow the previous analysis [2].

Online, the BMUI and RMUI chambers were used to tag muons by matching segments in the muon chambers with CTD-MVD tracks, as well as with energy deposits in the CAL consistent with the passage of a minimum-ionising particle (m.i.p.).

The different steps of the offline selection procedure are described in the following paragraphs. An event was accepted if it had two primary-vertex CTD-MVD tracks with invariant mass between 2 – 5 GeV. One track had to be identified in the inner muon chambers and matched to a m.i.p. cluster in the CAL. It was required to have a momentum greater than 1.8 GeV if it was in the rear region or a transverse momentum greater than 1.4 GeV if in the barrel region. The other track had to be matched to a m.i.p. cluster in the CAL and was required to have a transverse momentum greater than 0.9 GeV. Both tracks were restricted to the pseudorapidity region $|\eta| < 1.75$. To reject cosmic rays, events in which the angle between the two muon tracks was larger than 174° were removed.

In addition, events were required to have a calorimetric energy deposit larger than 1 GeV in a cone of 35° around the forward direction (excluding possible calorimeter deposits due to the decay muons). This requirement completely rejects exclusively produced J/ψ mesons, $ep \to epJ/\psi$. It also strongly suppresses the background from proton diffractive–dissociation, $ep \to eNJ/\psi$, because the low invariant mass hadronic system N can often (but not always) escape along the outgoing proton direction without any activity in the FCAL. A reduction of the remaining background is achieved by requiring the events to have, in addition to the two decay muon tracks, at least one additional track with transverse momentum larger than 250 MeV and pseudorapidity $|\eta| < 1.75$.

The ψ' production in proton diffractive–dissociation processes with the decay chain $J/\psi(\to \mu^+\mu^-)\ \pi^+\ \pi^-$ was identified in the selected data sample. For the bulk of these events only four charged tracks are visible in the detector. For the events with a $\mu^+\mu^-$ invariant mass, $m_{\mu\mu}$, in the interval [2.85, 3.30] GeV, and with exactly two additional primary–vertex tracks of opposite charge, the total invariant mass m_4 of the four tracks was evaluated. Events with a mass difference $m_4 - m_{\mu\mu}$ within ±60 MeV of the nominal mass difference $m_{\psi'} - m_{J/\psi} = 589$ MeV [21] were discarded. This topology was tagged only in 1.2% of the overall selected J/ψ sample and removed.

These requirements effectively select inelastic J/ψ and ψ' mesons. J/ψ and ψ' mesons from decays of b hadrons are also included in the data sample.

The kinematic region considered was defined by the inelasticity variable z and by the photon-proton centre-of-mass energy

$$W^2 = (P + q)^2, \tag{3}$$

where P and q are the four–momenta of the incoming proton and the exchanged photon, respectively. It was calculated using

$$W^2 = 2E_p(E - p_Z), \tag{4}$$

where $(E - p_Z)$, the difference between the energy and the momentum along the Z axis, is summed over all final-state energy-flow objects [22] (EFOs) which combine the information from calorimetry and tracking.

The inelasticity $z = \frac{P \cdot p_\psi}{P \cdot q}$ was determined as

$$z = \frac{(E - p_Z)_\psi}{(E - p_Z)}, \tag{5}$$

where ψ can be either a J/ψ or a ψ' meson, p_ψ is the four-momentum of the ψ and $(E - p_Z)_\psi$ was calculated using the two tracks forming the ψ.

In order to reject deep inelastic scattering, events were required to have $E - p_Z < 32$ GeV. This restricts the virtuality of the exchanged photon, $Q^2 = -q^2$, to $Q^2 \lesssim 1$ GeV^2, with a median of about 10^{-4} GeV^2. The elimination of deep inelastic scattering events was independently confirmed by searching for scattered electrons in the CAL [23]; none was found.

Table 1 summarises the various kinematic regions used for the presented measurements.

4 Monte Carlo models

The inelastic production of J/ψ and ψ' mesons was simulated using the HERWIG 6.100 [24] program, which generates direct photon events according to the LO diagrams of the photon–gluon fusion process, $\gamma g \to \psi g$. The processes are calculated in the framework of the CS model. The HERWIG MC provides in general a good description of the data. To improve the agreement further, the p_T spectrum was reweighted to the data. The average weight of the MC events with p_T around 1 GeV is 0.85. The average weight for $p_T > 4$ GeV is instead 1.8.

Diffractive production of J/ψ and ψ' mesons with proton dissociation was simulated with the EPSOFT [25] MC generator, which was tuned to describe such processes at HERA [26].

The PYTHIA 6.220 MC generator [27] was used to generate J/ψ and χ_c states from the resolved-photon process, with LO matrix elements computed in the CS model. The generator cross sections for the J/ψ and χ_c states are very similar. For the generation of the $\chi_{c1}(1P)$ and $\chi_{c2}(1P)$ mesons, only the $J/\psi\,\gamma$ decay channel was considered. The final state photon is at low energy, $O(400)$ MeV, basically indistinguishable from the remaining hadronic activity of the event. Hence the effective resolved-photon J/ψ contribution can be thought of as due to the genuine resolved-photon component plus the χ_c feed–down. The resolved ψ' contribution was neglected due to the small resolved-to-direct cross section ratio and to the additional reduction due to the $\psi' \to J/\psi X$ branching ratio.

The PYTHIA MC was also used to generate the production of J/ψ and ψ' mesons originating from b hadron decays, mostly from B-mesons. The following beauty-quark production processes were generated (according to the PYTHIA notation): direct, resolved, γ and proton excitation. The beauty-quark mass was set to 4.75 GeV and the branching ratios of the b hadrons to J/ψ and ψ' were set to the corresponding PDG [21] values.

All generated events were passed through a full simulation of the ZEUS detector based on GEANT 3 [28]. They were then subjected to the same trigger requirements and processed by the same reconstruction program as the data.

5 Signal determination and cross sections calculation

The invariant-mass spectrum of the muon pairs measured in the phase space region used in the determination of the ψ' to J/ψ cross section ratio, $60 < W < 190$ GeV and $0.55 < z < 0.9$, is shown in Fig. 2. A non-resonant background contribution, mostly due to hadrons misidentified as muons, is also visible. This contribution was estimated by fitting the product of a second-order polynomial and an exponential function to the region 2–2.75 and 3.8–5 GeV, outside the J/ψ and ψ' invariant-mass window. The number of J/ψ events was obtained by subtracting the number of background events, estimated from the fit procedure, from the total number of events inside the J/ψ invariant-mass window, 2.85–3.3 GeV. This procedure resulted in 11295 ± 114 J/ψ events. The same procedure applied to the ψ' invariant-mass window, 3.55–3.8 GeV, gave 448 ± 34 events.

Applying the same procedure to the phase space region used for the differential J/ψ cross section measurements, $60 < W < 190$ GeV, $0.1 < z < 0.9$ and $p_T > 1$ GeV, $12671 \pm$

161 J/ψ events were found. The fitting procedure described above was performed for each measurement bin presented in this paper.

The cross section for any observable, $\mathcal{O}$, was computed for each bin, i, using correction factors, $C_i(\mathcal{O})$, defined as $C_i(\mathcal{O}) = N_i^{\rm gen}(\mathcal{O})/N_i^{\rm rec}(\mathcal{O})$, where $N_i^{\rm gen}(\mathcal{O})$ is the number of events generated with the HERWIG MC and $N_i^{\rm rec}(\mathcal{O})$ is the number of the events reconstructed by the standard analysis chain. The factors $C_i(\mathcal{O})$ take into account the overall acceptance including the geometrical acceptance and the detector, trigger and reconstruction efficiencies. They also take into account bin-to-bin migrations.

For $0.9 < z < 1$, the events are largely diffractive. Therefore, the analysis of inelastic J/ψ production was restricted to the region $0.1 < z < 0.9$. In order to further suppress diffractive events, the transverse momentum of the J/ψ mesons had to fulfill $p_T > 1$ GeV. The remaining contamination was estimated by fitting the relative fractions of non-diffractive and diffractive events to the data z-distribution, using the HERWIG and EPSOFT MC simulations as templates. From this fit, the overall diffractive background contribution for $0.1 < z < 0.9$ is $4.6 \pm 1.6\%$.

In Fig. 3 the HERWIG and EPSOFT MC mixture, in the kinematic region $60 < W < 240$ GeV, $0.3 < z < 0.9$ and $p_T > 1$ GeV, is compared to the data: a reasonable description is found. The region $0.1 < z < 0.3$ was removed because not diffractive background is present at low z. The estimated diffractive background was subtracted bin by bin from the measured differential cross sections.

The cross sections measured in this analysis include also contributions from resolved-photon processes and from decays of beauty hadrons. Inelastic J/ψ production via the resolved-photon process has not been measured explicitly up to now in the photoproduction regime. QCD predictions, as well as the PYTHIA MC simulation described in Section 4, indicate that this contribution is largest at low z values. For $z < 0.1$, the expected size of this contribution can be larger than the direct-photon component. However, for $z > 0.1$, the resolved-to-direct photon production ratio is expected to be small. Since the acceptances obtained from the HERWIG and PYTHIA MC simulations are similar, the HERWIG MC alone was used for the overall acceptance corrections.

The contribution to the measured cross sections due to J/ψ originating from B meson decays was estimated using the inclusive beauty PYTHIA MC sample described in Section 4. The simulation predictions were scaled by a factor 1.11 according to the recent ZEUS measurement [29] of beauty photoproduction[3]. This leads to the estimation that on average 1.6%

[3]The scaling factors obtained in the measurements [29,30] vary between 1.11 and 1.84

of the observed J/ψ mesons originated from beauty hadron decays. The largest relative contribution, 4.5%, is in the kinematic region $0.1 < z < 0.3$ and $1 < p_T^2 < 2$ GeV^2. This component is not subtracted from the measured cross sections.

6 Systematic uncertainties

For all the measured quantities, the following sources of systematic uncertainties were investigated (their effects on the measured cross sections are given in parentheses):

- muon trigger and reconstruction efficiencies: the BMUI and RMUI muon chamber efficiencies were extracted from the data using muon pairs from elastic J/ψ events and from the process $\gamma\gamma \to \mu^+\mu^-$. These efficiencies take into account the full muon acquisition chain, from the online to the offline level and are known with a $\pm 5\%$ uncertainty (5% uniformly distributed in p_T and z);

- hadronic energy resolution: the W and z resolutions are dominated by the hadronic energy resolution affecting the quantity $(E - p_Z)$. The hadronic $(E - p_Z)$ resolution in the MC was smeared event by event by $\pm 20\%$, a conservative upper limit of a possible systematic difference between data and MC. This gave only small cross sections variations ($< 5\%$);

- HERWIG MC p_T spectrum: the p_T spectrum of the J/ψ mesons in the HERWIG MC simulation was varied within ranges allowed by the comparison between data and simulation and the correction factors were re-evaluated ($< 5\%$);

- J/ψ helicity distribution: the J/ψ helicity distribution can be described by two parameters λ and ν [31]. In the HERWIG MC these are set to zero. According to the direct measurement of the helicity parameters performed by ZEUS [12], all data points lie within the region of the λ-ν plane defined by $|\lambda| < 0.5$ and $|\nu| < 0.5$ with only a mild p_T or z dependence. Hence, as a systematic check, the HERWIG MC was reweighted varying independently λ and ν in the range ± 0.5 and the correction factors were re-evaluated ($5 - 10\%$ depending on the p_T and z region);

- diffractive simulation: the EPSOFT MC simulation parameters were varied within ranges allowed by the comparison between data and the EPSOFT MC simulation in the region $0.9 < z < 1$. The diffractive background was re-evaluated ($< 5\%$ at high z and low p_T, negligible elsewhere);

- diffractive subtraction: the relative fraction of inelastic and diffractive processes, as represented by the HERWIG and EPSOFT MC, was fixed by the procedure described in Section 5. It is known to a precision limited by the number of J/ψ events in the data and the process modeling by the MCs. The relative fractions were varied within ranges allowed by the comparison between data and simulation (up to 10% at high z and low p_T, negligible elsewhere);

- invariant–mass window: the $m_{\mu^+\mu^-}$ invariant–mass window used to estimate the number of J/ψ events above the non-resonant background was enlarged to $[2.8, 3.35]$ GeV and tightened to $[2.9, 3.3]$ GeV. For the ψ' to J/ψ cross section ratios, similar mass window variations were also applied for the ψ' signal (generally $< 5\%$, up to 10% at low z values where the number of expected and observed events is small and the non-resonant background is largest);

- additional track cut: the requirement of three tracks, including the two J/ψ decay muons, with transverse momentum larger than 250 MeV and pseudorapidity $|\eta| < 1.75$, was replaced by the requirement of five tracks with transverse momentum larger than 125 MeV, in the same pseudorapidity range. With this stronger requirement the diffractive J/ψ background and the diffractive ψ' contribution via the cascade decay $J/\psi(\rightarrow \mu^+\mu^-)\ \pi^+\ \pi^-$ are expected to vanish. Furthermore, a change in the overall multiplicity cut allows a test of how well the MC model reproduces the data in this respect. The MC mixture gives a fair description of the track multiplicity observed in the data. The cross sections were re-evaluated with the harder multiplicity cut (generally $< 5\%$, up to 20% in some bins at low z and high z high p_T).

All of the above individual sources of systematic uncertainty were added in quadrature.

The following sources would result in an overall small shift of the cross sections:

- the integrated luminosity determination gave an uncertainty of $\pm 1.9\%$;

- the $J/\psi \rightarrow \mu^+\mu^-$ branching ratio, $5.93 \pm 0.06\%$ [21], gave an uncertainty of $\pm 1\%$.

They were not included.

7 Results

7.1 ψ' to J/ψ cross section ratio

The ψ' to J/ψ cross section ratio was measured using the rates of $\psi' \to \mu^+\mu^-$ and $J/\psi \to \mu^+\mu^-$. The ratio was determined in the region $60 < W < 190$ GeV, $0.55 < z < 0.9$. The $p_T > 1$ GeV requirement was removed to maximise the available statistics. An increase of the diffractive background is expected. But under the assumption that this background contribution will be the same for the ψ' and J/ψ mesons it will cancel in the cross section ratio. The range $190 < W < 240$ GeV and $0.1 < z < 0.55$ was not included because the ψ' peak was not visible in this high W and low z region. The ψ' to J/ψ cross section ratio was computed in bins of W, z and p_T from

$$\frac{\sigma_i(\psi')}{\sigma_i(J/\psi)} = \frac{N_i^{2S}}{N_i^{1S}} \cdot \frac{C_i^{1S}}{C_i^{2S}} \cdot \frac{Br^{\mu}}{Br^{\mu'}} \cdot \left(1 - \frac{N_i^{2S}}{N_i^{1S}} \, \frac{C_i^{1S}}{C_i^{2S}} \, \frac{Br^{\mu}}{Br^{\mu'}} \, Br'\right)^{-1},$$

where, for the considered bin i, N_i^{1S} (N_i^{2S}) is the number of J/ψ (ψ') events observed, C_i^{1S} (C_i^{2S}) is the correction factor (see Section 5) computed using the HERWIG MC, Br^{μ} ($Br^{\mu'}$) is the J/ψ (ψ') muonic branching ratio and Br' is the $\psi' \to J/\psi \; X$ branching ratio. The values used are $Br^{\mu} = 5.93\%$, $Br^{\mu'} = 0.77\%$ and $Br' = 59.5\%$ [21]. With this technique, the cross section ratio was corrected for the $\psi' \to J/\psi \; (\to \mu^+\mu^-) \; X$ cascade decay.

Since NLO predictions are not available for ψ', only the LO CS model expectations can be compared to the data. In the CS model, the underlying production mechanism is the same for J/ψ and ψ', hence all cross section ratios should be largely independent of the kinematic variables. Using the values of Br^{μ} and $Br^{\mu'}$ given above, the expected ratio is 0.25 [4]. Since the NLO corrections, though being large, should be similar for J/ψ and ψ', the ratio at NLO is not expected to differ significantly from that at LO.

The results, shown in Fig. 4 and listed in Table 2, are dominated by the statistical uncertainties while most of the systematic uncertainties cancel in the ratio. The LO CS predictions agree reasonably well with the data.

7.2 J/ψ differential cross sections

The J/ψ differential cross sections presented here include the inelastic ψ' feed–down via the decay $\psi' \to J/\psi \; (\to \mu^+\mu^-) \; X$ and the contribution from b hadron decays. The ψ'

feed–down contributes about 15% and the b hadron decays 1.6% (see Section 5). The W range of the differential cross sections is $60 < W < 240$ GeV.

The differential cross sections $d\sigma/dp_T^2$ were measured in the range $1 < p_T^2 < 100$ GeV^2 for different z ranges. The results are listed in Table 3 and shown in Figs. 5 and 6. The predictions of a NRQCD calculation [7] are compared to the data in Fig. 5 and those based on the k_T–factorization approach [9] in Fig. 6.[4]

The differential cross sections $d\sigma/dz$ were measured in the range $0.1 < z < 0.9$ for different p_T ranges. The results are shown in Figs. 7 and 8 and listed in Table 4.

The present measurements are in agreement with the results obtained by the H1 collaboration [3] except in the region $z > 0.6$ and $p_T > 3$ GeV where the ZEUS cross sections are above the H1 measurements.

7.2.1 Comparison of NRQCD calculation

In Fig. 5 a prediction [7] performed in the NRQCD framework including direct and resolved photon processes is compared to the measured $d\sigma/dp_T^2$. The hard subprocesses take into account both CS and CO terms to NLO. The square of the renormalisation and factorisation scales used is $4 \cdot m_c^2 + p_T^2$, the charm quark mass, m_c, is set to 1.5 GeV and the strong coupling constant, $\alpha_s(M_Z)$, to 0.118. The NRQCD scale, connected to the colour-octet terms, is set to m_c. The CS contribution alone predicts cross sections significantly below the data[5] and fails to describe the data in all z regions shown here. Including CO terms give a dramatic improvement and leads to a rough agreement with the data. In general the calculation reproduces the steep drop of $d\sigma/dp_T^2$ with p_T^2, however, in the intermediate z range, $0.3 < z < 0.75$, the prediction rises less steeply than the data towards the smallest values of p_T^2.

In Fig. 7 the NRQCD predictions described above are compared to the measured $d\sigma/dz$. The predictions rise too steeply with z compared to the data, for all the p_T ranges.

[4] Both the NRQCD and the k_T–factorisation calculations do not include ψ' feed–down and b hadron decays, however these expected contributions are small compared to the uncertainties of the calculations.

[5] The NLO CS predictions [4] shown in the previous publication [2] were the first performed and used extreme values for the renormalisation and factorisation scales, with the effect of artificially increasing the normalisation of the predicted cross sections [32].

7.2.2 Comparison of k_T–factorisation approach

In Fig. 6 a prediction [9] performed in the k_T–factorisation approach is compared to the measured $d\sigma/dp_T^2$. The matrix elements are computed in the CS model using $m_c = 1.5$ GeV and $\alpha_s(M_Z) = 0.1232$. In the numerical calculation, the renormalisation and factorisation scales squared are set to $m_{J/\psi}^2 + p_T^2$ and $\hat{s} + Q_T^2$, respectively, where $\hat{s}$ is the four-momentum squared of the hard subprocess and Q_T is the transverse momentum of the initial parton. The unintegrated CCFM parton density [33] was selected. Using different sets of parton densities leads to changes in the prediction that are small with respect to the effects of scale variations already shown in Fig. 6. Thus this source of theoretical uncertainties was neglected. The k_T–factorisation prediction, with the values of m_c and α_s given above, provides a better description of the data than the NRQCD model.

The above k_T–factorisation predictions are compared to the differential cross sections $d\sigma/dz$ in Fig. 8. Here too the description is better than that of the NRQCD model. Note however that the k_T–factorisation model prediction suffers from large theoretical uncertainties, in particular at low p_T.

7.3 Momentum flow along and against the J/ψ direction

As pointed out by Brambilla et al. [1], the different colour flow in CS and CO hard subprocesses is expected to translate into different properties of the hadronic final state. In the photoproduction regime, the transverse momentum of the incoming photon is negligible. Thus in the CS model (see Fig. 1 (a)), at LO the J/ψ and the final state gluon are expected to be back to back. Hence, in this model, the momentum flow along the J/ψ direction, $\mathrm{P}_{\mathrm{along}}$, is expected to be small. The momentum flow against the J/ψ direction, $\mathrm{P}_{\mathrm{against}}$, should instead be driven by the hadronisation of the gluon. In the CO framework (see Fig. 1 (b)), no substantial difference is expected for $\mathrm{P}_{\mathrm{against}}$, compared to the CS framework. Instead, a contribution due to the soft gluons emitted by the $c\bar{c}$ pair forming the physical J/ψ state should be present. Hence, $\mathrm{P}_{\mathrm{against}}$ is again sensitive to gluon fragmentation while $\mathrm{P}_{\mathrm{along}}$ can shed light on the CO dynamics. As NRQCD framework MC generators are not presently available for *ep* collisions, only predictions of the CS model HERWIG MC are compared to the data.

The momentum flow analysis was performed for different p_T ranges. All track quantities described in the following were measured in the laboratory frame at the reconstruction level. Only primary vertex tracks with $p_T > 150$ MeV and $|\eta| < 1.75$ were selected. The J/ψ decay muon tracks were discarded. For each track whose component of momentum along

the J/ψ direction in the laboratory frame was positive, the component was included in P_{along}. If it was negative, it was included, in absolute value, in $P_{against}$. The data were restricted to $z > 0.3$ where the signal to background ratio is highest. The W and p_T ranges were $60 < W < 240$ GeV and $1 < p_T < 10$ GeV, respectively. The residual non-resonant background was subtracted for both $P_{against}$ and P_{along} variables using the shapes measured in the J/ψ side bands region and the normalisation obtained from the signal extraction procedure described in Section 5.

The $P_{against}$ (P_{along}) distribution, normalized to one, is shown in Fig. 9 (10). The prediction obtained from the HERWIG MC simulation (including detector simulation) is also shown. The $P_{against}$ distribution of the MC simulation shows a softer drop from the first to the second momentum bin than that of the data. This situation is reversed for the higher momenta values where HERWIG predicts a steeper decrease than that observed in the data. This behavior is seen for all p_T regions.

For the P_{along} distribution, shown in Fig. 10, a better agreement is found between the HERWIG MC prediction and the data.

8 Conclusions

A measurement of the inelastic photoproduction of J/ψ and ψ' mesons at HERA was presented. The ψ' to J/ψ cross section ratio was measured as a function of several kinematical observables. The constant value of 0.25 predicted by the LO CS model is in reasonable agreement with the data.

Double differential cross sections of inelastic J/ψ photoproduction were measured. A LO k_T calculation [9] using CS terms alone gives, within large normalisation uncertainties, a good description of the differential cross sections. However, for a better comparison with the data, a reduction of the theoretical uncertainties is very important.

A recent NLO calculation [7], using CS and CO terms in the collinear approximation, gives a rough description of the double differential cross sections. The same calculation with only CS terms is in strong disagreement with the data. This leads to the conclusion that CO terms are an essential ingredient for this particular model.

Predictions of the HERWIG MC, which includes only CS processes, were compared to the measured momentum flow along and against the J/ψ direction. HERWIG reproduces the fall off of the momentum distribution against the J/ψ direction as the momentum increases

but fails to describe the exact shape of this distribution. A better description is obtained along the J/ψ direction.

Acknowledgments

We appreciate the contributions to the construction and maintenance of the ZEUS detector of many people who are not listed as authors. The HERA machine group and the DESY computing staff are especially acknowledged for their success in providing excellent operation of the collider and the data analysis environment. We thank the DESY directorate for their strong support and encouragement. It is a pleasure to thank S. Baranov, M. Butenschön, B. Kniehl, A. Lipatov, F. Maltoni and N. Zotov for helpful discussions and for providing their predictions.

References

[1] N. Brambilla et al., Eur. Phys. J. **C 71**, 1534 (2011).

[2] ZEUS Coll., S. Chekanov et al., Eur. Phys. J. **C 27**, 173 (2003).

[3] H1 Coll., F. D. Aaron et al., Eur. Phys. J. **C 68**, 401 (2010).

[4] M. Krämer et al., Phys. Lett. **B 348**, 657 (1995);
M. Krämer, Nucl. Phys. **B 459**, 3 (1996).

[5] Chao-Hsi Chang, Rong Li and Jian-Xiong Wang, Phys. Rev. **D 80**, 34020 (2009).

[6] G.T. Bodwin, E. Braaten and G.P. Lepage, Phys. Rev. **D 51**, 1125 (1995). Erratum in Phys. Rev. **D 55**, 5853 (1997).

[7] M. Butenschön and B.A. Kniehl, Phys. Rev. Lett. **104**, 072001 (2010);
M. Butenschön and B.A. Kniehl, Phys. Rev. **D 84**, 051501(R) (2011).

[8] A.V. Lipatov and N.P. Zotov, Eur. Phys. J. **C 27**, 87 (2003).

[9] S.P. Baranov, A.V. Lipatov and N.P. Zotov, Eur. Phys. J. **C 71**, 1631 (2011).

[10] L.V. Gribov, E.M. Levin and M.G. Ryskin, Phys. Rep. **100**, 1 (1983);
E.M. Levin et al., Sov. J. Nucl. Phys. **53**, 657 (1991);
S. Catani, M. Ciafaloni and F. Hautmann, Nucl. Phys. **B 366**, 135 (1991);
J.C. Collins and R.K. Ellis, Nucl. Phys. **B 360**, 3 (1991).

[11] M. Ciafaloni, Nucl. Phys. **B 296**, 49 (1988);
S. Catani, F. Fiorani and G. Marchesini, Phys. Lett. **B 234**, 339 (1990).

[12] ZEUS Coll., S. Chekanov et al., Journal of High Energy Physics **12**, 007 (2009).

[13] ZEUS Coll., M. Derrick et al., Phys. Lett. **B 293**, 465 (1992).

[14] ZEUS Coll., U. Holm (ed.), *The ZEUS Detector*. Status Report (unpublished), DESY (1993), available on `http://www-zeus.desy.de/bluebook/bluebook.html`.

[15] N. Harnew et al., Nucl. Inst. Meth. **A 279**, 290 (1989);
B. Foster et al., Nucl. Phys. Proc. Suppl. **B 32**, 181 (1993);
B. Foster et al., Nucl. Inst. Meth. **A 338**, 254 (1994).

[16] A. Polini et al., Nucl. Inst. Meth. **A 581**, 656 (2007).

[17] M. Derrick et al., Nucl. Inst. Meth. **A 309**, 77 (1991);
A. Andresen et al., Nucl. Inst. Meth. **A 309**, 101 (1991);
A. Caldwell et al., Nucl. Inst. Meth. **A 321**, 356 (1992);
A. Bernstein et al., Nucl. Inst. Meth. **A 336**, 23 (1993).

[18] G. Abbiendi et al., Nucl. Inst. Meth. **A 333**, 342 (1993).

[19] J. Andruszków et al., Preprint DESY-92-066, DESY, 1992;
ZEUS Coll., M. Derrick et al., Z. Phys. **C 63**, 391 (1994);
J. Andruszków et al., Acta Phys. Pol. **B 32**, 2025 (2001).

[20] M. Helbich et al., Nucl. Inst. Meth. **A 565**, 572 (2006).

[21] K. Nakamura et al., Journal of Physics **G37**, 075021 (2010).

[22] ZEUS Coll., J. Breitweg et al., Eur. Phys. J. **C 1**, 81 (1998);
G.M. Briskin, *Diffractive Dissociation in ep Deep Inelastic Scattering*. Ph.D. Thesis, Tel Aviv University, Report DESY-THESIS 1998-036, 1998.

[23] H. Abramowicz, A. Caldwell and R. Sinkus, Nucl. Inst. Meth. **A 365**, 508 (1995).

[24] G. Marchesini et al., Comp. Phys. Comm. **67**, 465 (1992).

[25] M. Kasprzak, *Inclusive Properties of Diffractive and Non-diffractive Photoproduction at HERA*. Ph.D. Thesis, Warsaw University, Warsaw, Poland, Report DESY F35D-96-16, DESY, 1996.

[26] L. Adamczyk, *Vector Meson Photoproduction at Large Momentum Transfer at HERA*. Ph.D. Thesis, University of Mining and Metallurgy, Cracow, Poland, Report DESY-THESIS-1999-045, DESY, 1999.

[27] T. Sjöstrand et al., Comp. Phys. Comm. **135**, 238 (2001);
E. Norrbin and T. Sjöstrand, Eur. Phys. J. **C 17**, 137 (2000);
T. Sjöstrand, L. Lönnblad, and S. Mrenna, Preprint hep-ph/0108264, 2001.

[28] R. Brun et al., GEANT3, Technical Report CERN-DD/EE/84-1, CERN, 1987.

[29] ZEUS Coll., H. Abramowicz et al., Eur. Phys. J. **C 71**, 1659 (2011).

[30] ZEUS Coll., S. Chekanov et al., Journal of High Energy Physics **02**, 032 (2009).

[31] M. Butenschön and B.A. Kniehl, Phys. Rev. Lett. **107**, 232001 (2011).

[32] R. Brugnera, *Proceedings of the Europhysics Conference on High Energy Physics*. PoS (EPS-HEP 2009), available on
`http://pos.sissa.it/cgi-bin/reader/conf.cgi?confid=84`.

[33] H. Jung et al., Mod. Phys. Lett. **A 19**, 1 (2004).

$\psi^{'}$ to J/ψ cross section ratio: kinematic range		
$60 < W < 190$ GeV	$p_T > 0$ GeV	$0.55 < z < 0.9$
Differential cross sections: kinematic range		
$60 < W < 240$ GeV	$p_T > 1$ GeV	$0.1 < z < 0.9$
Momentum flow: kinematic range		
$60 < W < 240$ GeV	$1 < p_T < 10$ GeV	$0.3 < z < 0.9$

Table 1: *The different kinematic regions used in the measurement of the $\psi^{'}$ to J/ψ cross section ratio, J/ψ differential cross sections and momentum flow along and against the J/ψ direction.*

p_T range (GeV)	$\langle p_T \rangle$ (GeV)	$\sigma(\psi^{'})/\sigma(J/\psi)$
$0.0 - 1.0$	0.63	$0.262 \pm 0.043^{+0.003}_{-0.014}$
$1.0 - 1.75$	1.35	$0.317 \pm 0.049^{+0.010}_{-0.005}$
$1.75 - 5.0$	2.68	$0.263 \pm 0.041^{+0.030}_{-0.002}$
W range (GeV)	$\langle W \rangle$ (GeV)	$\sigma(\psi^{'})/\sigma(J/\psi)$
$60 - 95$	81.42	$0.368 \pm 0.054^{+0.052}_{-0.042}$
$95 - 120$	108.03	$0.409 \pm 0.057^{+0.006}_{-0.015}$
$120 - 190$	149.11	$0.218 \pm 0.040^{+0.026}_{-0.015}$
z range	$\langle z \rangle$	$\sigma(\psi^{'})/\sigma(J/\psi)$
$0.55 - 0.70$	0.62	$0.250 \pm 0.043^{+0.014}_{-0.015}$
$0.70 - 0.80$	0.75	$0.289 \pm 0.040^{+0.007}_{-0.019}$
$0.80 - 0.90$	0.85	$0.344 \pm 0.054^{+0.036}_{-0.008}$

Table 2: *Cross section ratio of $\psi^{'}$ to J/ψ as a function of p_T, W and z in the kinematic region $60 < W < 190$ GeV and $0.55 < z < 0.9$. In the quoted ratios, the first uncertainty is statistical and the second is systematic.*

z range	p_T^2 range (GeV^2)	$\langle p_T^2 \rangle$ (GeV^2)	$d\sigma/dp_T^2$ (nb/GeV^2)	$d\sigma(b \to J/\psi)/dp_T^2$ (nb/GeV^2)
$0.10 - 0.30$	$1.0 - 2.0$	1.46	$1.03 \pm 0.13^{+0.18}_{-0.15}$	0.05
	$2.0 - 3.0$	2.47	$0.86 \pm 0.12^{+0.10}_{-0.17}$	0.04
	$3.0 - 4.5$	3.67	$0.410 \pm 0.079^{+0.055}_{-0.068}$	0.029
	$4.5 - 7.0$	5.64	$0.127 \pm 0.047^{+0.020}_{-0.027}$	0.018
	$7.0 - 10.0$	8.37	$0.052 \pm 0.030^{+0.022}_{-0.008}$	0.012
	$10.0 - 14.0$	11.62	$0.056 \pm 0.017^{+0.009}_{-0.006}$	0.007
	$14.0 - 20.0$	16.34	$0.0329 \pm 0.0081^{+0.0029}_{-0.0066}$	0.0035
	$20.0 - 40.0$	26.50	$0.0069 \pm 0.0018^{+0.0010}_{-0.0008}$	0.0012
	$40.0 - 100.0$	56.69	$0.00092 \pm 0.00037^{+0.00018}_{-0.00026}$	0.00013
$0.30 - 0.45$	$1.0 - 2.0$	1.47	$1.32 \pm 0.10^{+0.21}_{-0.16}$	0.02
	$2.0 - 3.0$	2.45	$0.823 \pm 0.081^{+0.094}_{-0.101}$	0.018
	$3.0 - 4.5$	3.70	$0.492 \pm 0.060^{+0.071}_{-0.075}$	0.013
	$4.5 - 7.0$	5.64	$0.190 \pm 0.032^{+0.024}_{-0.028}$	0.010
	$7.0 - 10.0$	8.35	$0.111 \pm 0.019^{+0.014}_{-0.013}$	0.006
	$10.0 - 14.0$	11.77	$0.062 \pm 0.011^{+0.010}_{-0.007}$	0.004
	$14.0 - 20.0$	16.49	$0.0349 \pm 0.0052^{+0.0030}_{-0.0035}$	0.0021
	$20.0 - 40.0$	27.96	$0.0065 \pm 0.0012^{+0.0009}_{-0.0008}$	0.0007
	$40.0 - 100.0$	54.05	$0.00095 \pm 0.00019^{+0.00014}_{-0.00007}$	0.00009
$0.45 - 0.60$	$1.0 - 2.0$	1.45	$2.20 \pm 0.09^{+0.25}_{-0.25}$	-
	$2.0 - 3.0$	2.47	$1.38 \pm 0.08^{+0.15}_{-0.16}$	-
	$3.0 - 4.5$	3.69	$0.84 \pm 0.05^{+0.12}_{-0.10}$	-
	$4.5 - 7.0$	5.65	$0.424 \pm 0.029^{+0.054}_{-0.058}$	-
	$7.0 - 10.0$	8.35	$0.249 \pm 0.017^{+0.029}_{-0.029}$	-
	$10.0 - 14.0$	11.79	$0.121 \pm 0.010^{+0.013}_{-0.013}$	-
	$14.0 - 20.0$	16.60	$0.0505 \pm 0.0048^{+0.0046}_{-0.0051}$	0.0007
	$20.0 - 40.0$	26.70	$0.0106 \pm 0.0011^{+0.0009}_{-0.0009}$	0.0004
	$40.0 - 100.0$	55.86	$0.00122 \pm 0.00020^{+0.00013}_{-0.00015}$	0.00003
$0.60 - 0.75$	$1.0 - 2.0$	1.45	$2.80 \pm 0.10^{+0.35}_{-0.32}$	-
	$2.0 - 3.0$	2.47	$2.07 \pm 0.09^{+0.23}_{-0.23}$	-
	$3.0 - 4.5$	3.70	$1.10 \pm 0.05^{+0.13}_{-0.13}$	-
	$4.5 - 7.0$	5.60	$0.680 \pm 0.030^{+0.084}_{-0.084}$	-
	$7.0 - 10.0$	8.38	$0.286 \pm 0.017^{+0.031}_{-0.036}$	-
	$10.0 - 14.0$	11.93	$0.153 \pm 0.010^{+0.015}_{-0.016}$	-
	$14.0 - 20.0$	16.92	$0.0532 \pm 0.0044^{+0.0051}_{-0.0050}$	-
	$20.0 - 40.0$	27.0	$0.0123 \pm 0.0011^{+0.0011}_{-0.0011}$	-
	$40.0 - 100.0$	55.77	$0.00112 \pm 0.00018^{+0.00010}_{-0.00022}$	-
$0.75 - 0.90$	$1.0 - 2.0$	1.45	$2.39 \pm 0.13^{+0.51}_{-0.35}$	-
	$2.0 - 3.0$	2.45	$1.77 \pm 0.11^{+0.44}_{-0.23}$	-
	$3.0 - 4.5$	3.66	$1.17 \pm 0.07^{+0.16}_{-0.15}$	-
	$4.5 - 7.0$	5.64	$0.716 \pm 0.039^{+0.087}_{-0.092}$	-
	$7.0 - 10.0$	8.31	$0.369 \pm 0.023^{+0.042}_{-0.045}$	-
	$10.0 - 14.0$	11.77	$0.166 \pm 0.012^{+0.016}_{-0.020}$	-
	$14.0 - 20.0$	16.66	$0.0650 \pm 0.0058^{+0.0053}_{-0.0087}$	-
	$20.0 - 40.0$	26.22	$0.0139 \pm 0.0013^{+0.0012}_{-0.0025}$	-
	$40.0 - 100.0$	54.0	$0.00093 \pm 0.00018^{+0.00007}_{-0.00018}$	-

Table 3: *Measured J/ψ differential photoproduction cross sections in the kinematic region $0.1 < z < 0.9$ and $60 < W < 240$ GeV as a function of the squared transverse momentum of the J/ψ mesons in bins of inelasticity z. In the quoted cross sections, the first uncertainty is statistical and the second is systematic. The bin center values $\langle p_T^2 \rangle$ and the expected, but not subtracted, beauty contribution (estimated through the* PYTHIA *MC) are also given in the table. The beauty contribution is only given when its value is above 1% with respect to the corresponding measured differential photoproduction cross section.*

p_T range (GeV)	z range	$\langle z \rangle$	$d\sigma/dz$ (nb)	$d\sigma(b \to J/\psi)/dz$ (nb)
$1.0 - 2.0$	$0.10 - 0.30$	0.21	$11.5 \pm 1.0^{+1.5}_{-1.9}$	0.6
	$0.30 - 0.45$	0.37	$17.3 \pm 1.0^{+2.3}_{-2.2}$	0.4
	$0.45 - 0.60$	0.52	$29.9 \pm 0.9^{+3.3}_{-3.4}$	-
	$0.60 - 0.75$	0.67	$40.2 \pm 1.0^{+4.4}_{-4.5}$	-
	$0.75 - 0.90$	0.82	$36.6 \pm 1.2^{+6.6}_{-4.9}$	-
$2.0 - 3.0$	$0.10 - 0.30$	0.21	$1.94 \pm 0.78^{+0.31}_{-0.45}$	0.43
	$0.30 - 0.45$	0.37	$6.42 \pm 0.71^{+0.78}_{-0.81}$	0.28
	$0.45 - 0.60$	0.52	$12.4 \pm 0.6^{+1.5}_{-1.5}$	0.8
	$0.60 - 0.75$	0.67	$18.6 \pm 0.6^{+2.2}_{-2.2}$	-
	$0.75 - 0.90$	0.82	$19.4 \pm 0.8^{+2.4}_{-2.3}$	-
$3.0 - 4.5$	$0.10 - 0.30$	0.20	$2.55 \pm 0.47^{+0.36}_{-0.28}$	0.30
	$0.30 - 0.45$	0.38	$3.51 \pm 0.41^{+0.37}_{-0.37}$	0.26
	$0.45 - 0.60$	0.52	$6.61 \pm 0.37^{+0.66}_{-0.72}$	0.08
	$0.60 - 0.75$	0.68	$7.79 \pm 0.35^{+0.74}_{-0.75}$	-
	$0.75 - 0.90$	0.82	$9.29 \pm 0.46^{+0.84}_{-1.15}$	-
> 4.5	$0.10 - 0.30$	0.21	$1.01 \pm 0.20^{+0.10}_{-0.13}$	0.16
	$0.30 - 0.45$	0.38	$1.31 \pm 0.18^{+0.15}_{-0.12}$	0.24
	$0.45 - 0.60$	0.52	$1.98 \pm 0.17^{+0.16}_{-0.16}$	0.08
	$0.60 - 0.75$	0.67	$2.11 \pm 0.16^{+0.18}_{-0.19}$	-
	$0.75 - 0.90$	0.82	$2.16 \pm 0.18^{+0.18}_{-0.49}$	-

Table 4: *Measured J/ψ differential photoproduction cross sections in the kinematic region $p_T > 1$ GeV and $60 < W < 240$ GeV as a function of the inelasticity z in bins of transverse momentum of the J/ψ meson. In the quoted cross sections, the first uncertainty is statistical and the second is systematic. The bin center values $\langle z \rangle$ and the expected, but not subtracted, beauty contribution (estimated through the* PYTHIA *MC) are also given in the table. For further details see Table 3.*

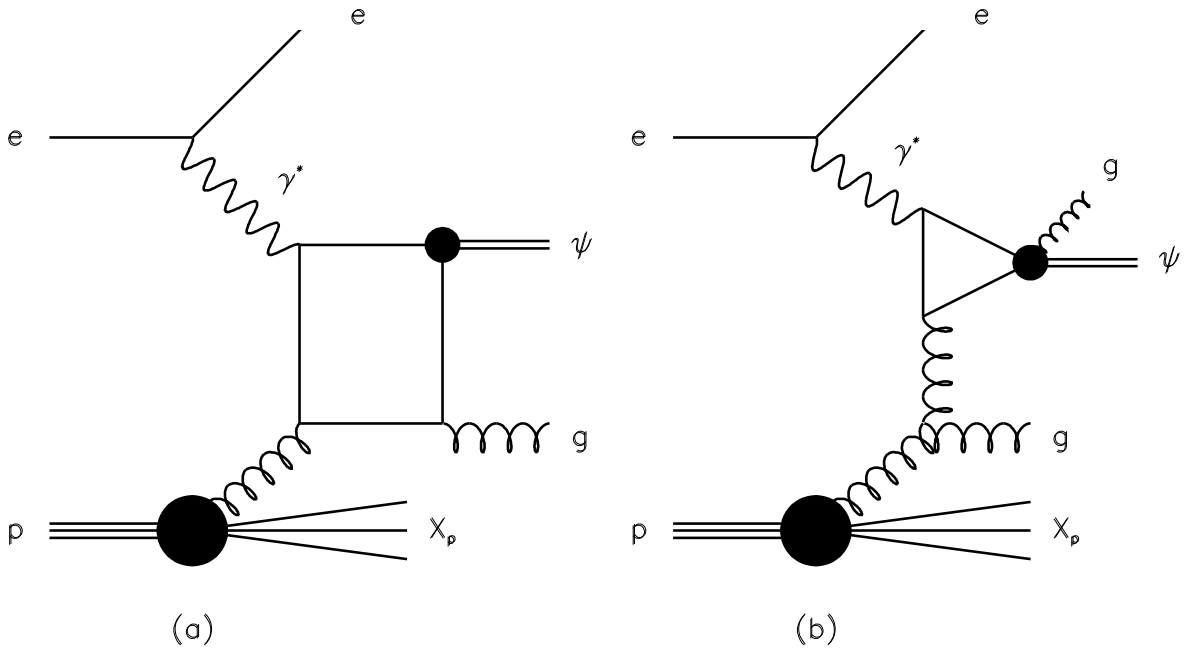

Figure 1: *Examples of direct photon-processes at leading-order in (a) the colour-singlet and (b) the colour-octet frameworks.*

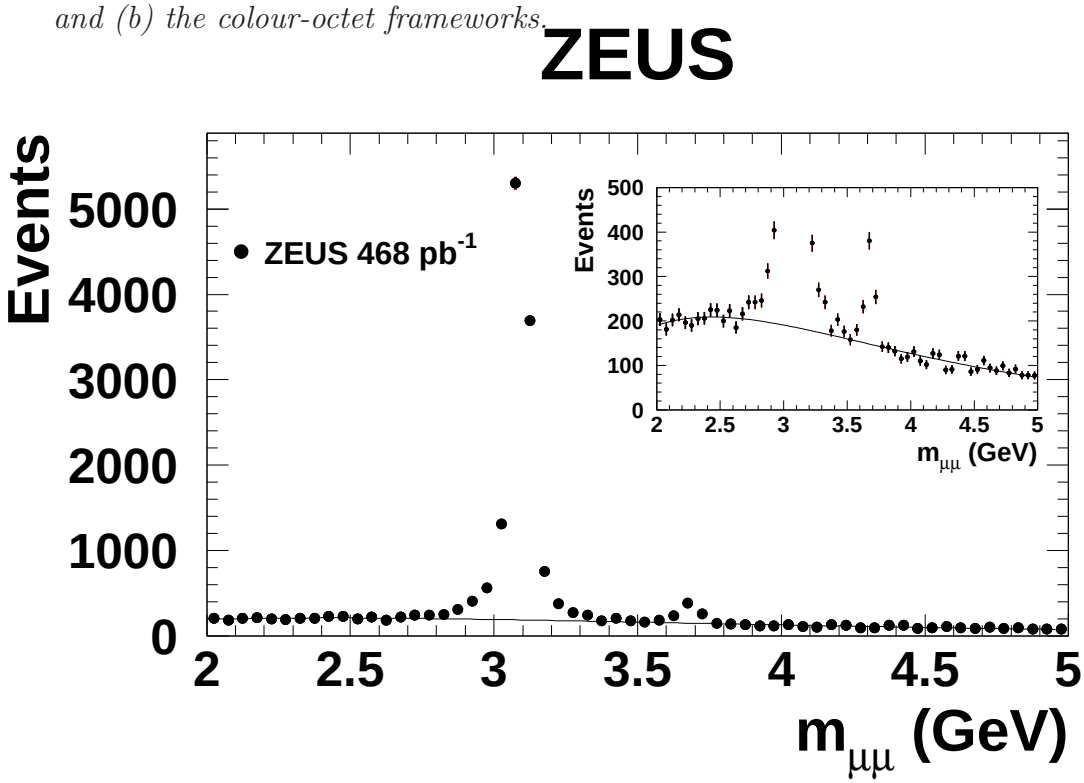

Figure 2: *Invariant-mass distribution, $m_{\mu\mu}$, in the kinematic region $0.55 < z < 0.9$ and $60 < W < 190$ GeV. The continuous line shows the estimated background contribution (for further details see the text). The right insert highlights the ψ' mass peak.*

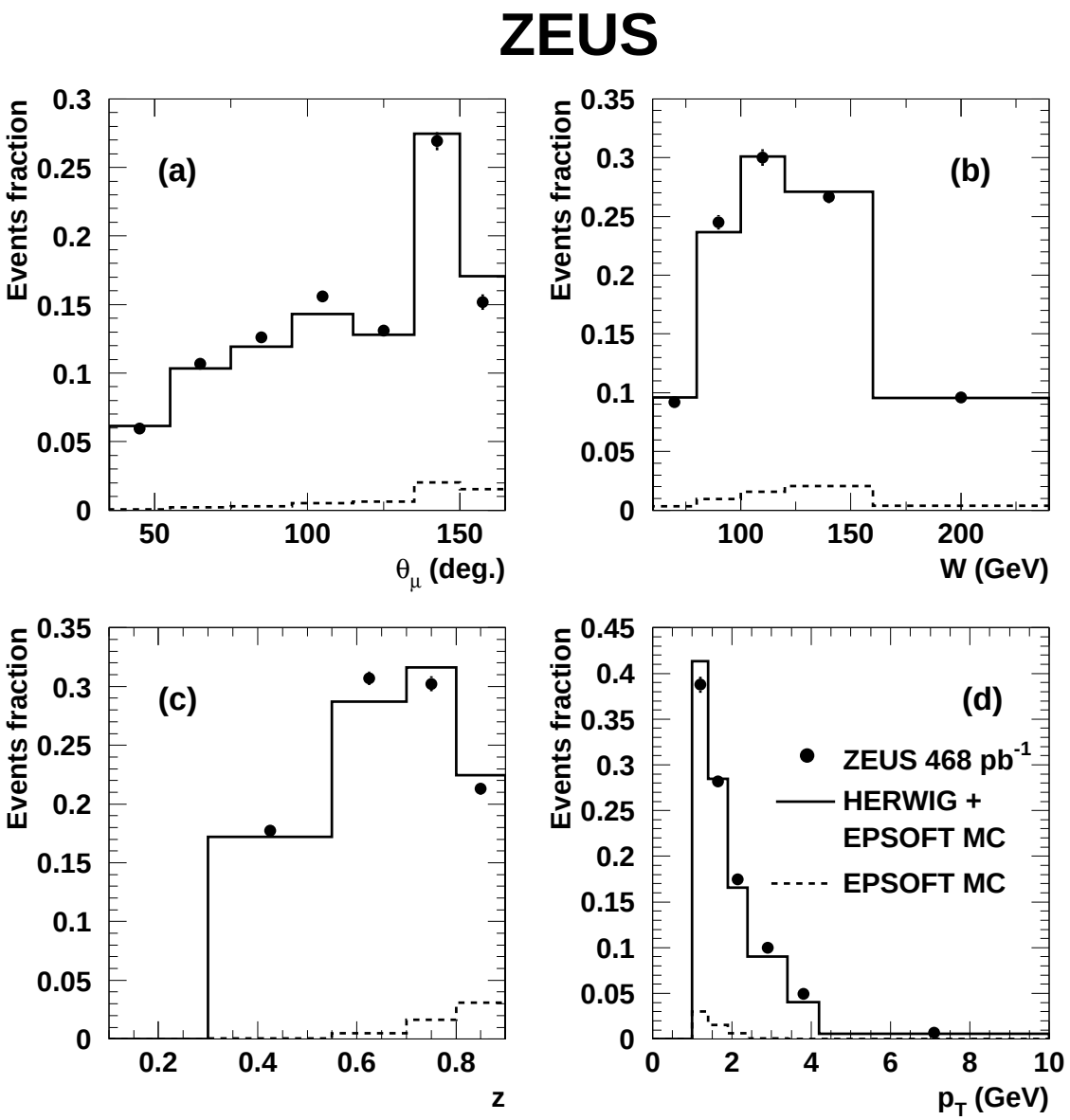

Figure 3: *J/ψ events fraction measured in the kinematic region $0.3 < z < 0.9$, $60 < W < 240$ GeV and $p_T > 1$ GeV as a function of (a) the polar angle θ_μ of the muon tracks, (b) W, (c) the inelasticity z and (d) the J/ψ p_T. The data are shown as points. The error bars are the statistical uncertainties. The sum of the* HERWIG *and* EPSOFT *MC predictions, according to the relative fraction described in the text and normalised to the data are also shown (continuous lines). The* EPSOFT *MC component is shown separately (dashed lines).*

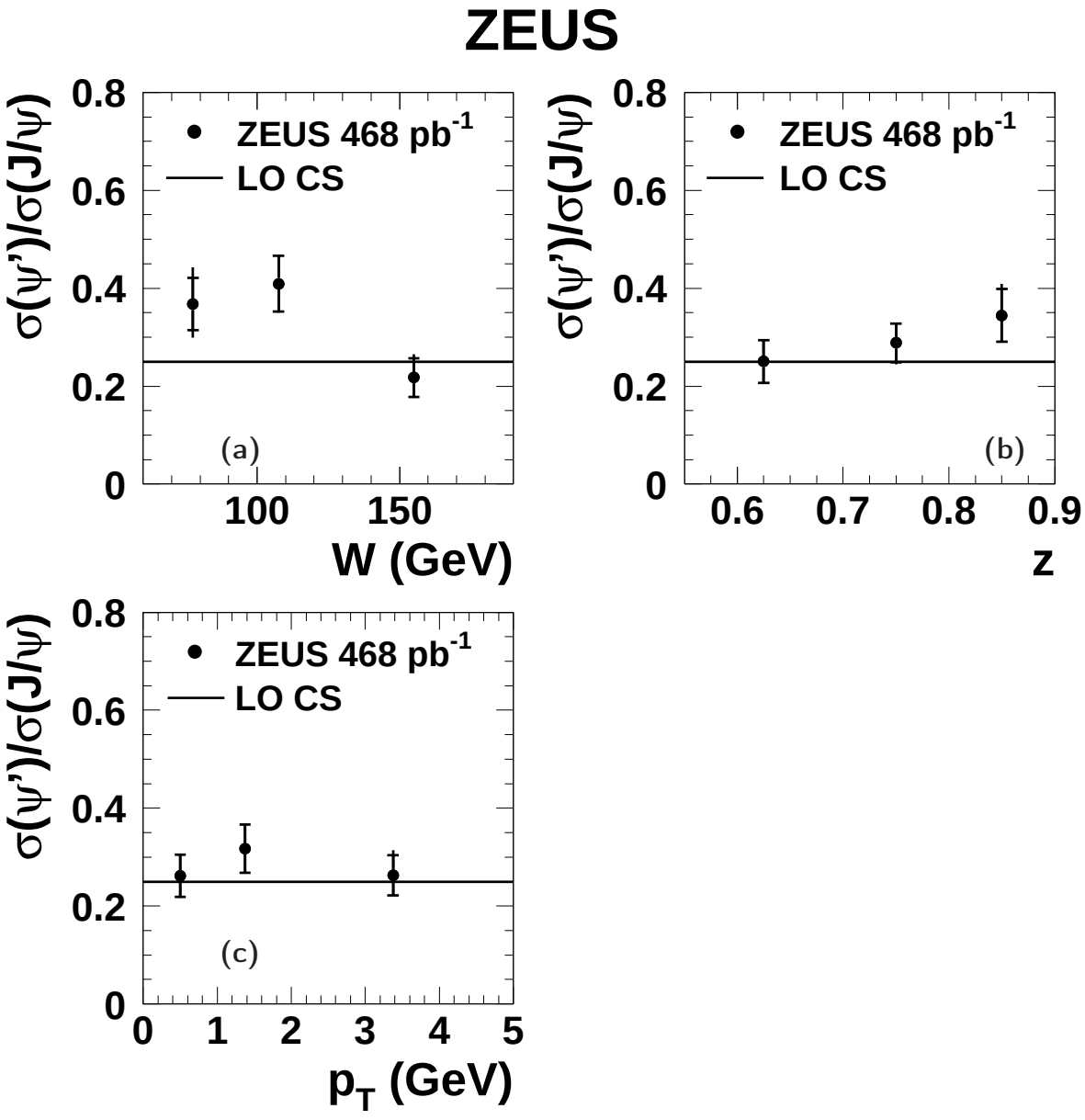

Figure 4: *ψ' to J/ψ photoproduction cross section ratio measured in the kinematic region $0.55 < z < 0.9$ and $60 < W < 190$ GeV as a function of (a) W, (b) the inelasticity z and (c) p_T. The data are shown as points. The inner error bars are the statistical uncertainties, while the outer error bars show the statistical and systematic uncertainties added in quadrature. The leading-order colour-singlet model expectation (horizontal lines) is also shown.*

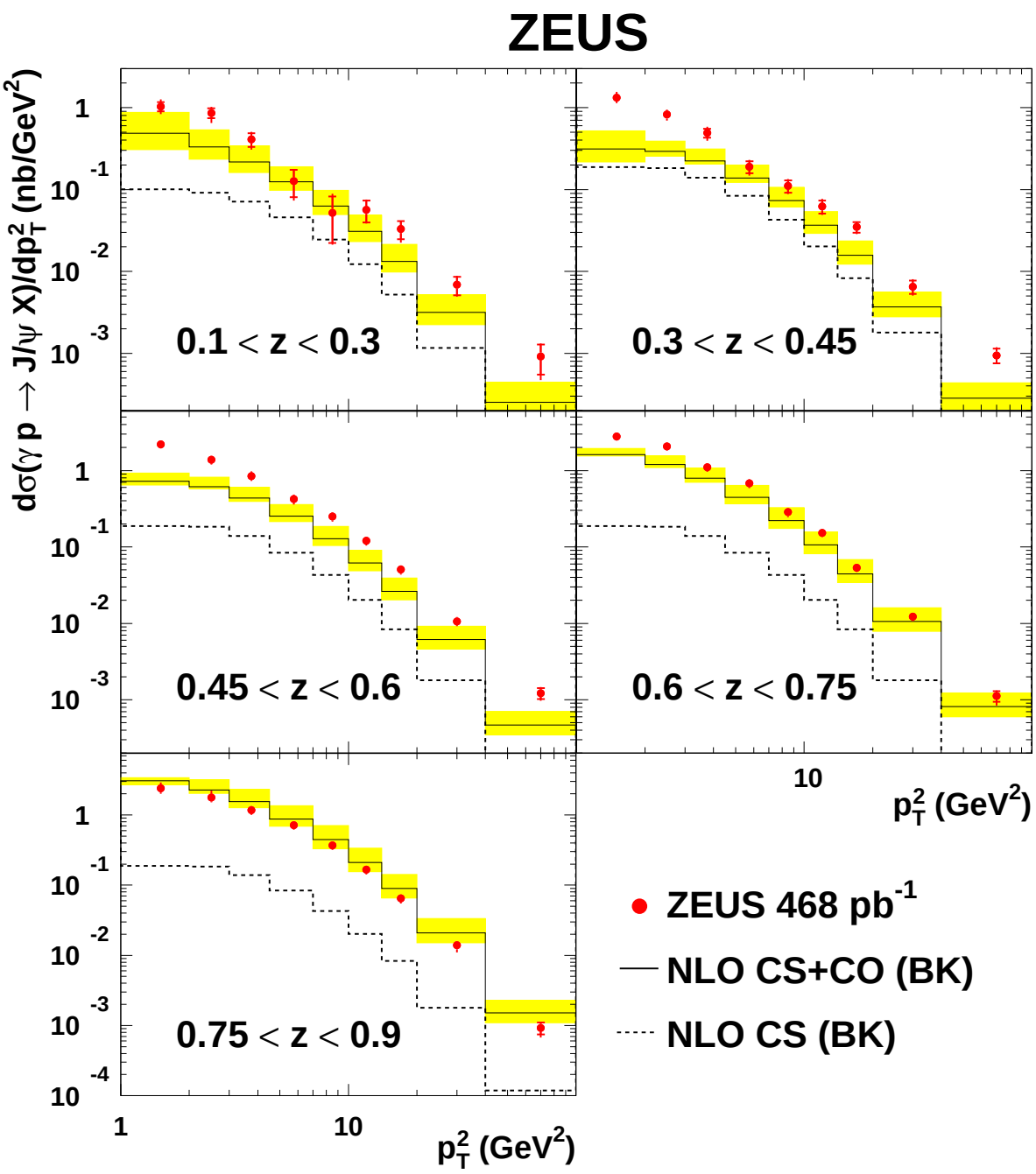

Figure 5: *Differential cross sections $d\sigma/dp_T^2$ measured in 5 different z ranges. The measurement is performed in the kinematic region $60 < W < 240$ GeV and $p_T > 1$ GeV. The data are shown as points. The inner (outer) error bars represent the statistical (total) uncertainties. The solid lines show the NLO CS+CO (BK) prediction [7] obtained in the non-relativistic QCD framework. The uncertainties are indicated by the band. The colour-singlet model contribution is presented separately as the dashed lines.*

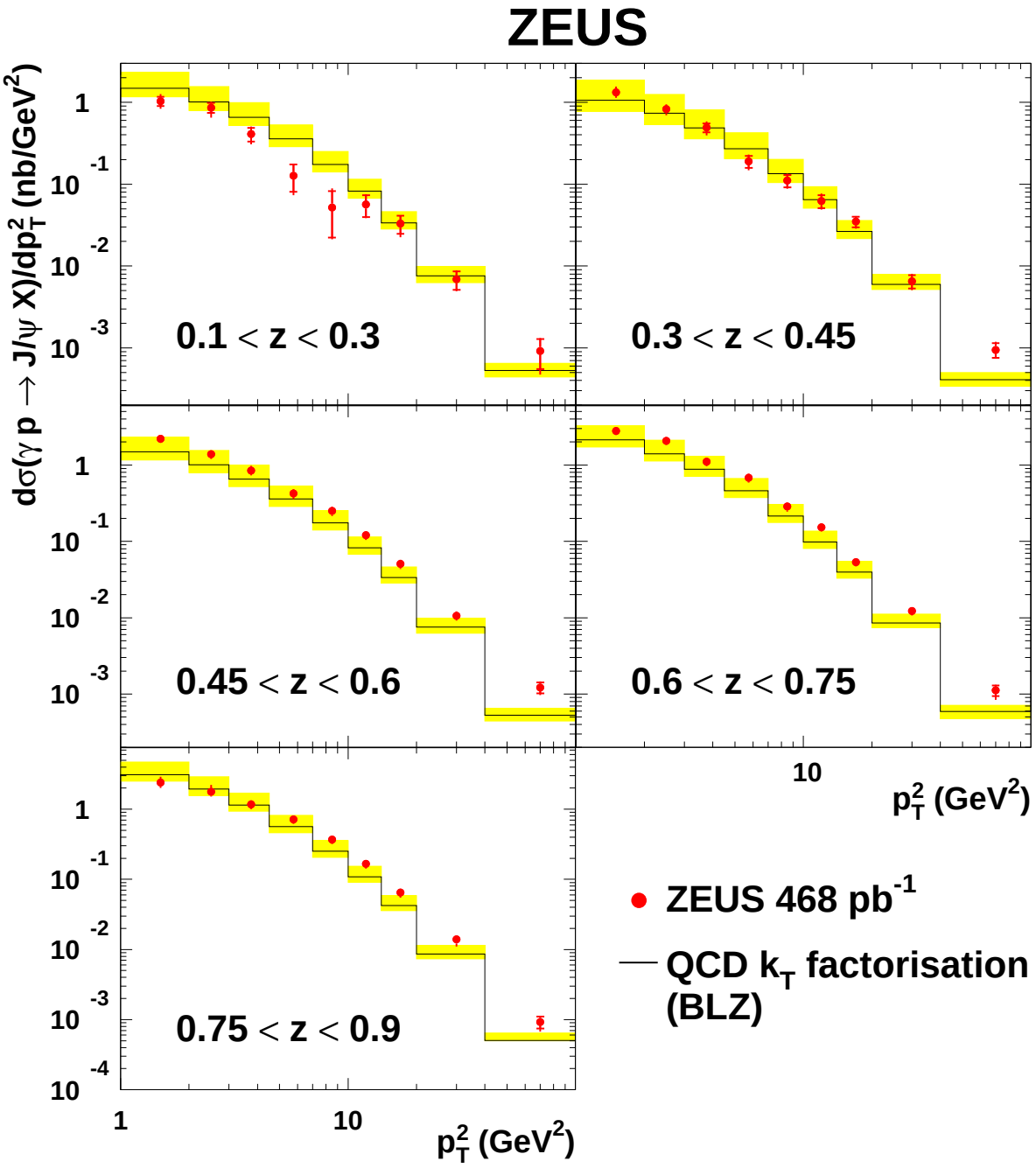

Figure 6: *Differential cross sections $d\sigma/dp_T^2$ measured in 5 different z ranges. The measurement is performed in the kinematic region $60 < W < 240$ GeV and $p_T > 1$ GeV. The data are shown as points. The inner (outer) error bars represent the statistical (total) uncertainties. The solid lines show the k_T–factorisation (BLZ) prediction [8,9]. The uncertainties are indicated by the band.*

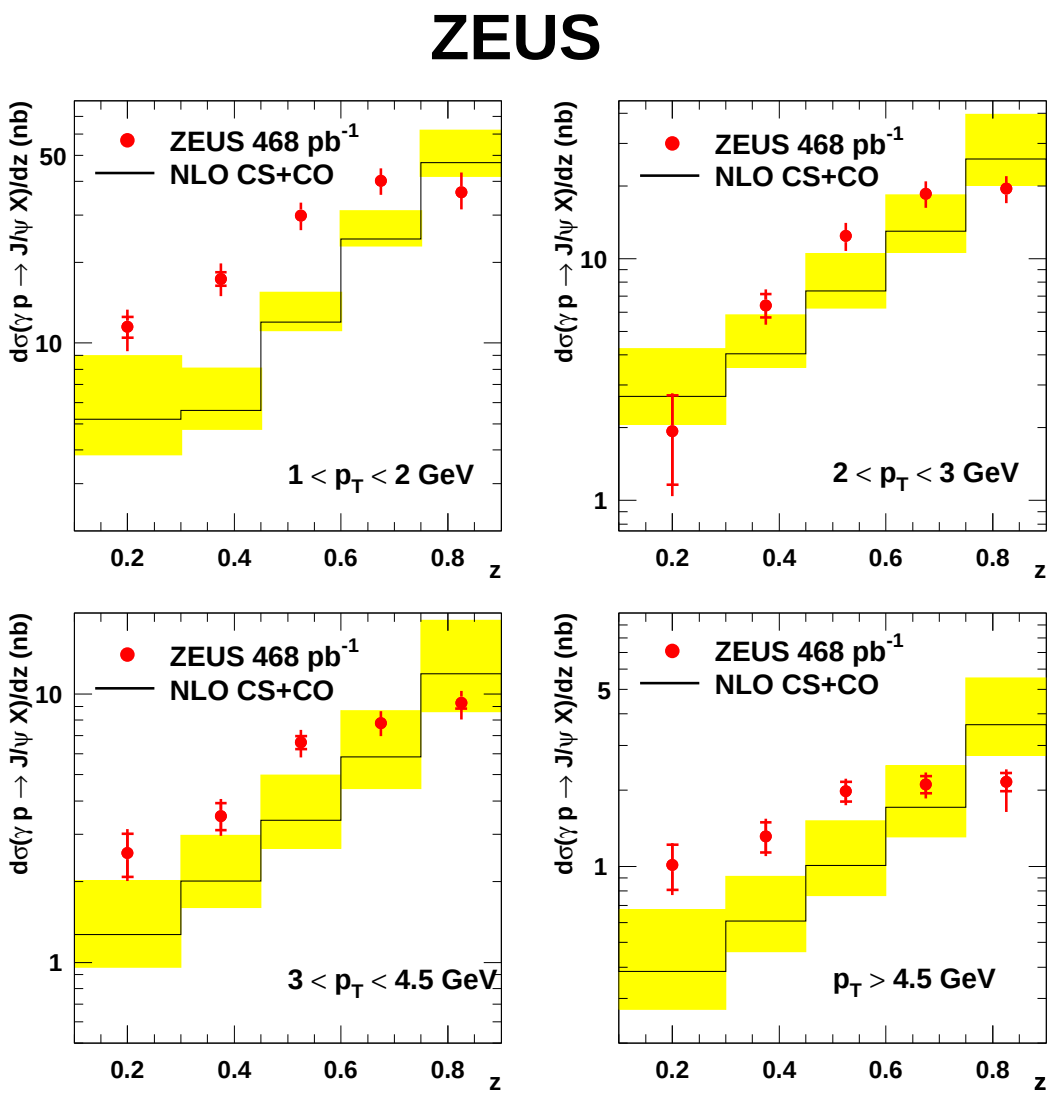

Figure 7: *Differential J/ψ cross sections $d\sigma/dz$ measured in 4 different p_T ranges. The measurement is performed in the kinematic region $60 < W < 240$ GeV and $0.1 < z < 0.9$. The data are shown as points. The inner (outer) error bars represent the statistical (total) uncertainties. The solid lines show the NLO CS+CO (BK) prediction [7] obtained in the non-relativistic QCD framework. The uncertainties are indicated by the band.*

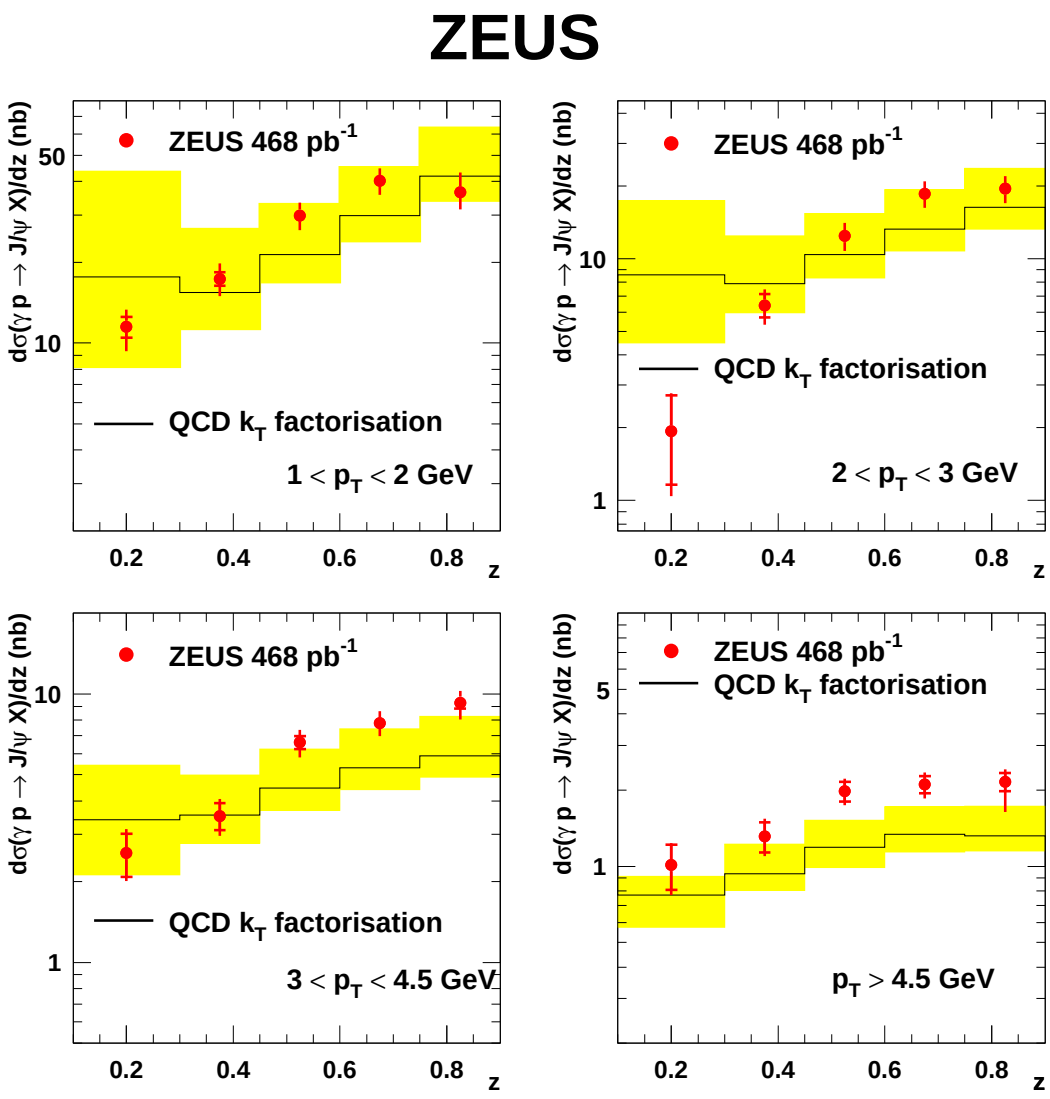

Figure 8: *Differential J/ψ cross sections $d\sigma/dz$ measured in 4 different p_T ranges. The measurement is performed in the kinematic region $60 < W < 240$ GeV and $0.1 < z < 0.9$. The data are shown as points. The inner (outer) error bars represent the statistical (total) uncertainties. The solid lines show the k_T–factorisation (BLZ) prediction [8, 9]. The uncertainties are indicated by the band.*

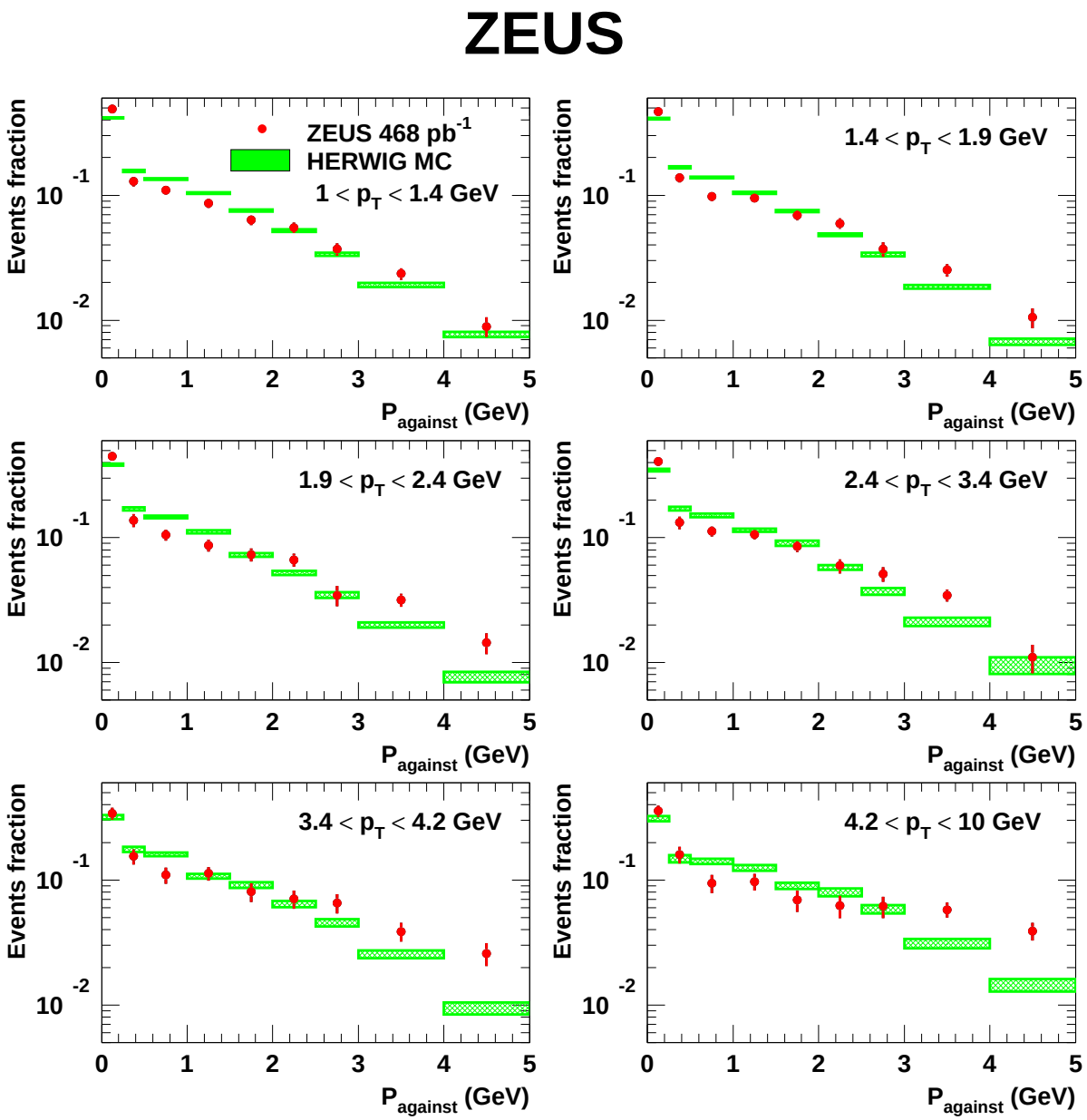

Figure 9: *Momentum flow against the J/ψ direction of flight in the laboratory frame, $P_{against}$, for different p_T ranges. The distributions are normalized to unity and are not corrected for detector acceptance. The measurement is performed in the kinematic region $60 < W < 240$ GeV and $0.3 < z < 0.9$. The data are shown as points with error bars indicating their uncertainties. The predictions obtained from the* HERWIG *MC are also shown as rectangular shaded boxes. The height of these boxes represents the uncertainties of the prediction.*

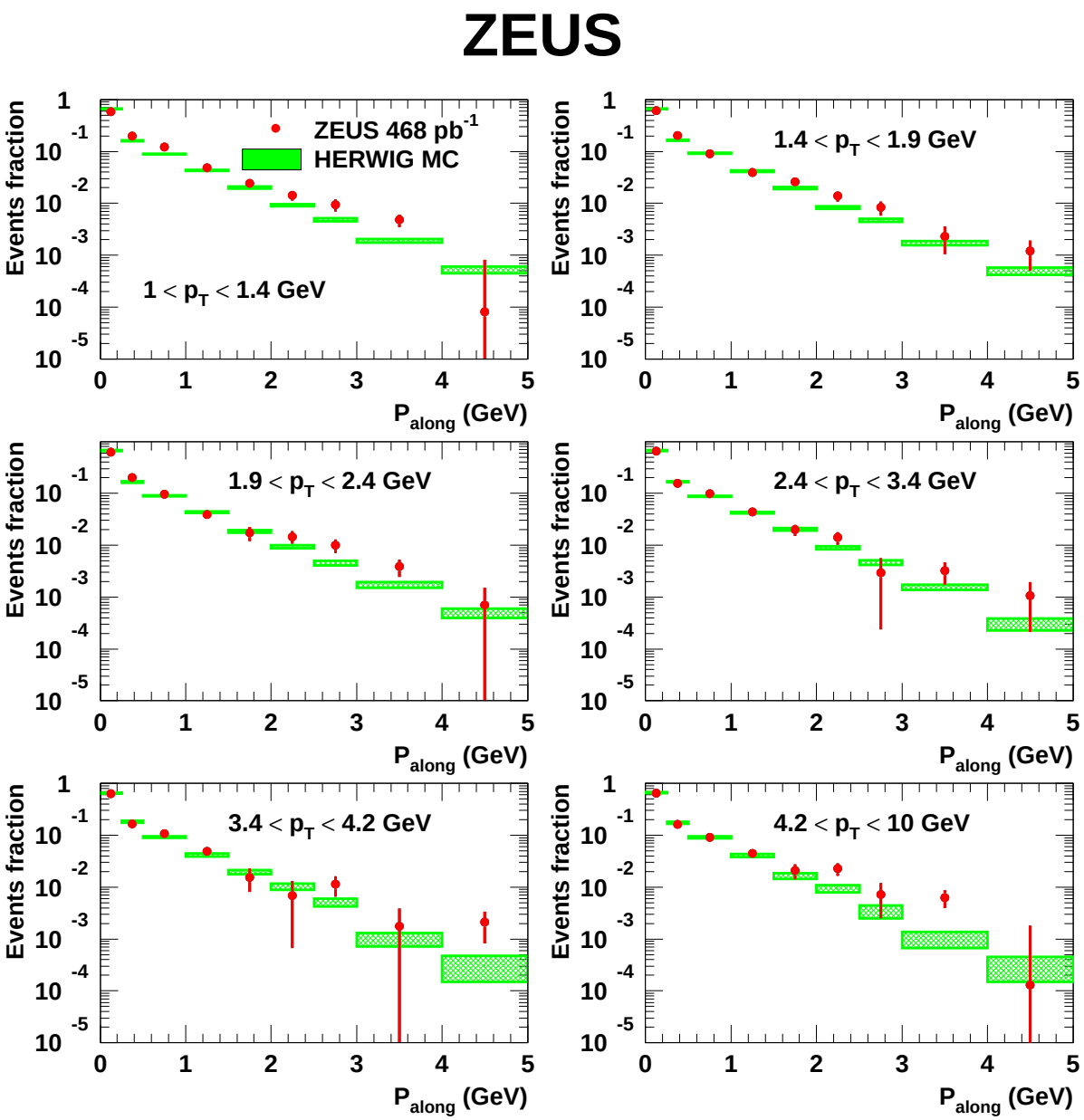

Figure 10: *Momentum flow along the J/ψ direction of flight in the laboratory frame, P_{along} , for different p_T ranges. The distributions are normalized to unity and are not corrected for detector acceptance. The measurement is performed in the kinematic region $60 < W < 240$ GeV and $0.3 < z < 0.9$. The data are shown as points with error bars indicating their uncertainties. The predictions obtained from the* HERWIG *MC are also shown as rectangular shaded boxes. The height of these boxes represents the uncertainties of the prediction.*